

Special acoustical role of pinna simplifying spatial target localization by the brown long-eared bat *Plecotus auritus*

Xin Ma^{1,2,*}, Sen Zhang¹, Zheng Dong¹, Hongwang Lu³, Jinke Li⁴, and Weidong Zhou^{5,*}


¹*School of Information Science and Engineering, Shandong University, Qingdao, Shandong 266237, China*

²*Shenzhen Research Institute, Shandong University, Shenzhen, Guangdong 518057, China*

³*School of Physics, Shandong University, Jinan, Shandong 250100, China*

⁴*Department of Mathematics, University of Kansas, Lawrence, Kansas 66045, USA*

⁵*School of Microelectronics, Shandong University, Jinan, Shandong 250101, China*

 (Received 27 May 2020; revised 24 August 2020; accepted 29 September 2020; published 15 October 2020)

Echolocating bats locate a target by sonar. The performance of this system is related to the shape of the binaural conformation in bats. From numerical predictions, it was found that in a central frequency band, the orientation of a strong sidelobe is shifted nearly linearly in the vertical direction. Inspired by this, the authors built an accurate wide-scope elevation estimation system by constructing a pair of erect artificial pinnae and realized simultaneous elevation and azimuth estimation by constructing a pair of orthogonal pinnae. By demonstrating the simplicity of spatial target echolocation, the authors showed that only two independent single-output neural networks were needed for either elevation or azimuth estimation. This method could be applied to imitate any other mammal species with similar pinna directivity patterns to facilitate and improve an artificial echolocation system.

DOI: [10.1103/PhysRevE.102.040401](https://doi.org/10.1103/PhysRevE.102.040401)

A large number of mammals, including humans, possess intricate outer-ear shapes that diffract incoming sounds in a direction- and frequency-specific manner [1]. This attracts much attention from researchers, who have focused on navigation and target localization [2–6]. A bat possesses excellent navigation and target localization capabilities that have been proved to be related to outer-ear shapes [7–10].

There have been many studies on the relationship between the external ear and three-dimensional spatial directionality. For example, Wotton *et al.* conducted a physical experiment to measure the directionality of the external ear of the big brown bat (*Eptesicus fuscus*) and found that notches and peaks in transfer function varied systematically with changes in elevation [11]. Later, they had shown this by conducting a series of bat behavior experiments [12,13]. Wotton and Simmons [12] and Müller [14] also pointed out that the tragus in the external ear of the big brown bat or the brown long-eared bat (*Plecotus auritus*) is related to vertical sound localization. Chiu and Moss [15] also demonstrated this by conducting a behavioral experiment based on the behavior of big brown bats.

Müller *et al.* [16] took advantage of finite-element model simulation and found that in the aural directivity pattern of the pinna of the brown long-eared bat, the main lobe (the lobe with the most energy in the frequency band) always points towards the tip of the ear, and its orientation remains almost unchanged with frequency. The first sidelobe (the lobe with the secondmost energy in the frequency band) sweeps along the vertical direction in the scope of the ventral direction; for this reason, it is also called the ventral sidelobe. Although

many researchers have established quantitative links between the actual directivity of a mammalian pinna and the generated spatial information, how to use this information in practical applications is still a huge issue. For spatial target localization, the most direct way is to construct an identification pattern for each location [17,18]. In other words, if the transfer function of every direction is taken as one category, the question of localization can be solved as a pattern recognition problem. Because the aural directivity patterns of bat ears at different frequencies are generally not the same, according to the reciprocity principle, the echo intensity composition of spatial targets located in a certain direction will vary according to the frequency used by the bat. Therefore, the echo direction can be determined by detecting the strength composition patterns of different frequencies, which can be considered equivalent to transfer functions in different directions. However, this approach consumes excessive computational resources.

In this study, both numerical simulations and physical experiments have been conducted. By numerical simulation of the pinna of the long-eared bat [Fig. 1(a)], a strong ventral sidelobe was found to shift almost linearly in the vertical direction as the frequency changed from 34 to 60 kHz [Fig. 1(b)]. The -3 dB contours [Fig. 1(c)] of the strong ventral sidelobe were wider in the horizontal direction and narrower in the longitudinal direction. This helped establish a quantitative link between the actual directivity of a pinna and the generated spatial information in the long-eared bat, which became the mechanism for the proposed three-dimensional (3D) spatial target localization method and served to construct a simple spatial target localization approach.

Because the aural directivity patterns are obtained by a single pinna, the aural directivity pattern of each ear is

*max@sdu.edu.cn; wdzhou@sdu.edu.cn

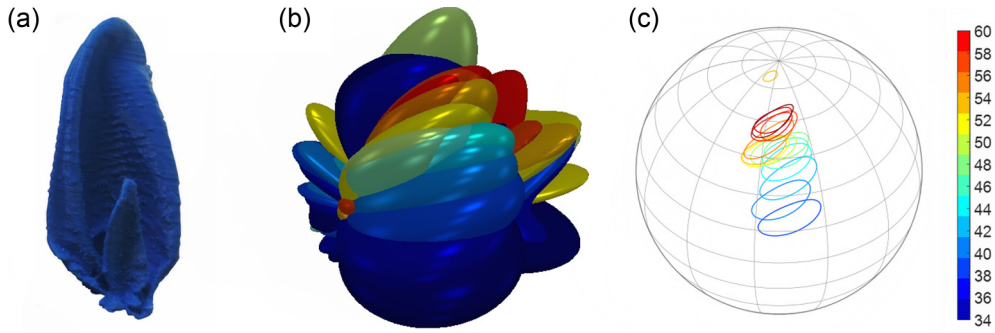


FIG. 1. Pinna of the brown long-eared bat and its aural spatial directivity: (a) an outline of a pinna model from the brown long-eared bat; (b) aural spatial directivity pattern visualized by three-dimensional isosurfaces of beam gain; (c) -3 dB contours of a ventral sidelobe (first sidelobe), which performs a frequency-driven scan in the band from 34 to 60 kHz. The scale bar here also applies to the isosurface blobs (b).

relatively independent. Obviously, different binaural topologies can generate different aural directivity pattern combinations in space. Therefore, two forms of binaural topology were designed to imitate spatial target localization by the brown long-eared bat: the first one consisted of parallel erect pinnae [Fig. 2(a)], whose -3 dB contours in the strong ventral sidelobe had the form shown in Fig. 2(b).

The other geometry is orthogonal pinnae [Fig. 2(c)], whose -3 dB contours in the strong ventral sidelobe are shown in Fig. 2(d). Theoretically, for parallel erect pinnae, the acoustic feature can equivalently widen the scope of action only in the horizontal direction, whereas the spatial information remains stable and the rate of change in the aural directivity pattern with frequency is more obvious in the vertical direction. This means that much more information is obtained in the vertical direction than in the horizontal direction. For the orthogonal pinnae, in the overlapping regions, the amount of information is the same in both orthogonal directions, as well as in the horizontal and vertical directions.

For purposes of comparison, a similar experiment was conducted on artificial pinnae of the brown long-eared bat

[Fig. 3(a)] for spatial target localization in an experimental chamber [8 m (length) \times 6 m (width) \times 3.6 m (height)] with no sound insulation. The measurement target was a small rubber ball with a diameter of 11 cm suspended by a string [Fig. 3(a)]. The signal acquisition and processing device was a signal acquisition card (PXIe-6358 and PXIe-1082; National Instruments, Austin, Texas, USA; sampling at 100 KS/s) that enabled multichannel synchronous signal acquisition. An ultrasonic loudspeaker was set up to emit a batlike frequency-modulated (FM) signal to imitate the pulse emitted by the brown long-eared bat.

The artificial pinnae were produced using a 3D printer according to a 3D digital model obtained based on pinna samples taken from the carcass of a brown long-eared bat. To avoid damage during assembly and to provide room for the insertion of a microphone at the location of the external auditory meatus, the artificial batlike ears were printed three times larger than the original ear. A single ultrasonic microphone (SPU0410LR5H-QB; Knowles Electronics, Itasca, Illinois, USA) was inserted at the base (root) of each artificial ear, and an ultrasonic loudspeaker (UltraSound Gate Player BL Light; Avisoft Bioacoustics e.K., Glienicke, Germany) was located below the pinnae. The entire apparatus was fixed on a rotating platform to form an artificial batlike sonar system. To

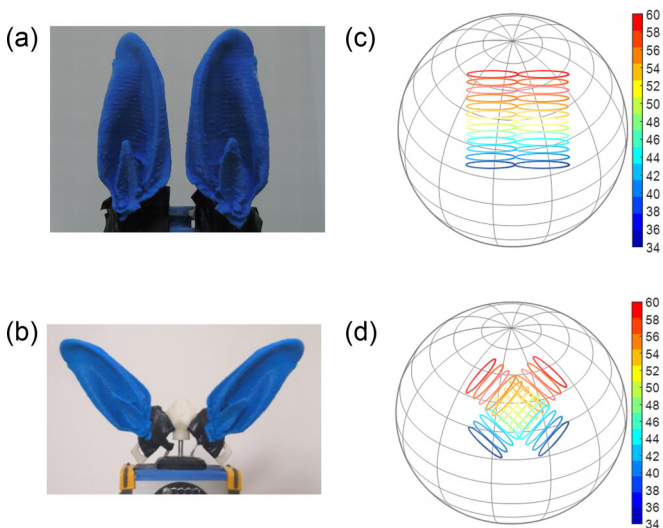


FIG. 2. Artificial parallel erect pinnae (a) and their ideal -3 dB contours (b); artificial orthogonal pinnae (c) and their ideal -3 dB contours (d).

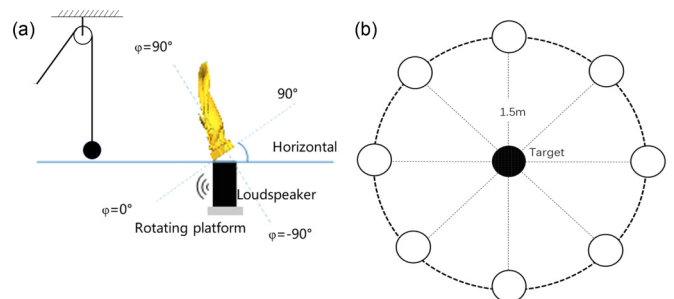


FIG. 3. Definition of elevation angle (a) and locations of the target and device during training and testing; the elevation was changed by altering the height of the rubber ball used as the target. (b) The artificial batlike ear device was moved in turn to each of the eight locations (white circles) surrounding the spherical target to locate and obtain the data. The data obtained at each site served as test data, and the data obtained at other sites served as training data in the eightfold cross-validation experiments.

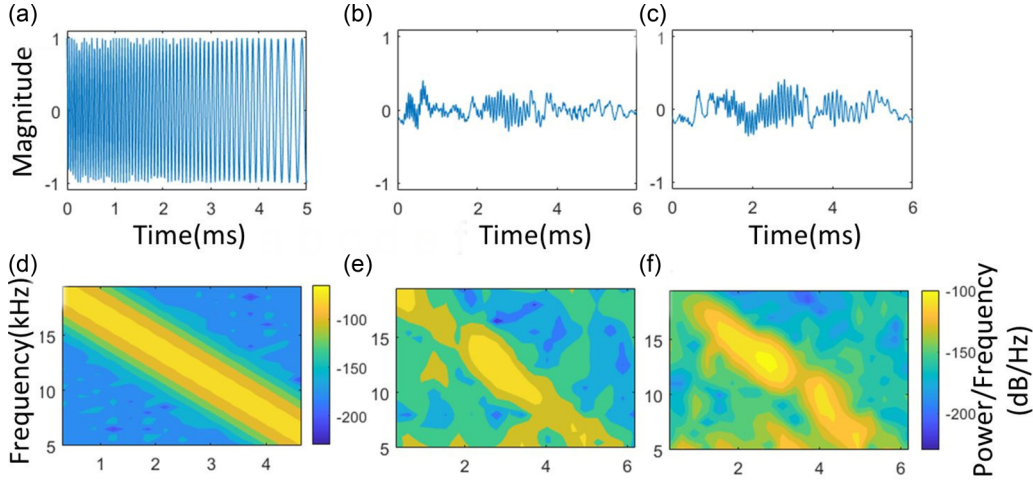


FIG. 4. Example of a signal emitted by the loudspeaker and echoes received by the two ears: (a), (b), (c) emitted signal and echoes received by left and right microphones; (d), (e), (f) spectrograms for the emitted signal and the echoes received by the left and right microphones.

perform eightfold cross validation and to separate the test data and location from the training data and location, the artificial batlike sonar was moved in turn to each of the eight locations [Fig. 3(b)] to obtain the echo signal. When measurements were conducted, the horizontal distances between the target and the sonar were maintained at 1.5 m as illustrated in Fig. 3(b). The relative direction between the target and the artificial batlike sonar was adjusted by controlling the height of the target [Fig. 3(a)] and the horizontal rotation of the sonar. In other words, elevation was adjusted by altering the height of the rubber ball used as the target, and the azimuth was adjusted by rotating the platform horizontally. The signal acquisition card was set to the two-channel synchronous signal acquisition working mode to collect binaural signals in a synchronous manner.

Because the signal emitted by the brown long-eared bat is a type of FM pulse signal with 60 kHz down to 20 kHz bandwidth and sweeping down in frequency, the loudspeaker was set to emit a similar FM pulse signal sweeping down in frequency [Fig. 4(a)], but with 20 kHz down to 5 kHz bandwidth according to the scale model principle. [In fact, the lower bound was slightly extended, as shown in Fig. 4(d)]. The duration of the batlike FM pulse signal was 5 ms with a 0.08 ms rise time and a 0.08 ms fall time. Its time-frequency intensity (spectrogram) is shown in Fig. 4(d). The echoes received by the two artificial pinnae are shown in Figs. 4(b) and 4(c), and their corresponding spectrograms are shown in Figs. 4(e) and 4(f). We can see the spectrogram energy of the emitted signal or the echoes received by the two pinnae was mainly concentrated near the diagonal line [Figs. 4(d)–(f)].

Due to the circuit noise in the instruments and equipment and the non-sound-insulation chamber, the signal-to-noise ratio (SNR) of the emitted signal was about 22 dB. Because the loudspeaker and pinna used in our experiments were both directional, when the target deviation was large relative to

the azimuthal midline the echo signal became weaker, or in other words, the echo signal-to-noise ratio became lower. In all measurement directions, the best echo SNR was close to 18 dB and appeared in the target direction facing the loudspeaker; the worst was 10 dB when the target was located at the marginal azimuth.

Considering the characteristic of sweeping FM signal, the feature extractions are based on the time-frequency representation [19] of the echoes. The effective signals received by the pair of ultrasonic microphones were transferred into a time-frequency representation to yield

$$X_n(e^{j\omega}) = \sum_{m=-\infty}^{\infty} x(m)W(n-m)e^{-j\omega m}, \quad (1)$$

where $x(n)$ is the signal received after the endpoint detection process and $W(n)$ is the window function, which shifts the sound signal by a step length on the time axis. We used Hamming windows with a length of 1 ms (100 samples) as the window function and the shift step was half of the window length. The spectrogram representation X can be calculated as

$$X = |X_n(e^{j\omega})|^2, \quad (2)$$

for which energy in the emitted pulse signal or the echo was concentrated near that diagonal line. Hence, a threshold was set to suppress the effects of interference components while maintaining the value constant on or near the diagonal line in the spectrogram. The spectrogram was then restricted to one vector by summing the values along the frequency channels. After the experiment, a time-frequency representation with length T was transformed into a vector with n elements, as described in Eq. (3). In the present experiment, $n = 30$, and the vectors were connected from the left and right echo signals to obtain one vector with 60 elements as the classifier input.

$$\begin{aligned}
 X = \begin{pmatrix} x_{11} & x_{12} & \cdots & x_{1T} \\ \vdots & \vdots & \ddots & \vdots \\ x_{n1} & x_{n2} & \cdots & x_{nT} \end{pmatrix} &\xrightarrow{\text{set threshold}} \begin{pmatrix} 0 & \cdots & x_{1i} & x_{1i+1} & \cdots & x_{1i+d} & \cdots & 0 \\ \vdots & \vdots & \vdots & \ddots & \ddots & \ddots & \ddots & \vdots \\ 0 & \cdots & \cdots & \cdots & x_{ni+n-1} & x_{ni+n} & \cdots & x_{ni+n-1+d} \end{pmatrix} \\
 &\xrightarrow{\text{truncate}} \begin{pmatrix} x_{1i} & x_{1i+1} & \cdots & x_{1i+d} & \cdots & 0 \\ \vdots & \ddots & \ddots & \ddots & \ddots & \vdots \\ 0 & \cdots & x_{ni+n-1} & x_{ni+n} & \cdots & x_{ni+n-1+d} \end{pmatrix} \\
 &\xrightarrow{\Sigma} \begin{pmatrix} X_1 \\ \vdots \\ X_n \end{pmatrix}. \tag{3}
 \end{aligned}$$

The back-propagation (BP) feedforward neural networks used in all the tasks had the same structure [20], which consisted of an input layer with 60 neurons (30 + 30, i.e., the features extracted from the echo signals for the left and right artificial ears were fed directly into the network), a hidden layer with nine neurons, and an output layer with one output neuron. The three layers were fully connected in the BP neural network [21]. Tan-sigmoid and pure linear were selected as the activation functions in the hidden layer and the output layer, respectively. In the training phase, the neural network learned the characteristics of the time-frequency patterns reflected by the target at different angles (elevations or azimuths). The network was trained using the Levenberg-Marquardt optimization algorithm. After training, the time-frequency patterns generated from untrained ultrasonic echoes were fed into the network. The outputs were linearly transformed into activities between 0.05 (minimum) and 0.95 (maximum). During estimation, the output neuron activities were linearly retransformed according to the activity functions and then were used as the angle estimates for the respective inputs to each task.

To obtain reliable results, eightfold cross validation (the data from seven sites were used as training data, and the data from the remaining site were used as testing data in turn) was conducted. The sonar device [illustrated in Fig. 3(a)] was moved to each of the eight sites, with the small ball used as the target located at the center, and the horizontal distance between the ball and each maintained at 1.5 m as indicated in Fig. 3(b). At each site, data collection was performed in 19×8 directions for parallel erect pinnae experiments (-90° to 90° with 10° step size in azimuth and 20° to 55° with 5° step size in elevation) and in 9×9 directions for orthogonal pinnae experiments (-28° to 28° in azimuth, 12° to 68° in elevation, and both with a 7° step size).

To clarify the wide-angle effect of the elevation estimation, statistics were calculated for different azimuth ranges. For example, the values of $-N^\circ$ to $+N^\circ$ in parallel erect pinnae experiments for estimating elevation [Fig. 5(a)] represented the limited angle range, and both the training and test data came from the same range. In estimating the azimuth [Fig. 5(b)], only one limited range in the elevation direction (20° to 55°) was used.

For parallel erect pinnae, the average precision was nearly 100% within the limited azimuth range from -20° to $+20^\circ$,

while the average accuracy exceeded 90% when the azimuth limit angle ranged from -60° to $+60^\circ$, and the average accuracy exceeded 80% even when the limit angle of the azimuth was -90° to $+90^\circ$ [Fig. 5(a)]. These findings illustrated the good wide-angle effect on elevation estimation and the high accuracy in the middle direction of the azimuth, which are essential for target detection. In contrast, the average accuracy of azimuth estimation was only about 40% within the limited angle of elevation range from 20° to 55° [Fig. 5(b)]. This shows that the azimuth estimates were clearly not as good as

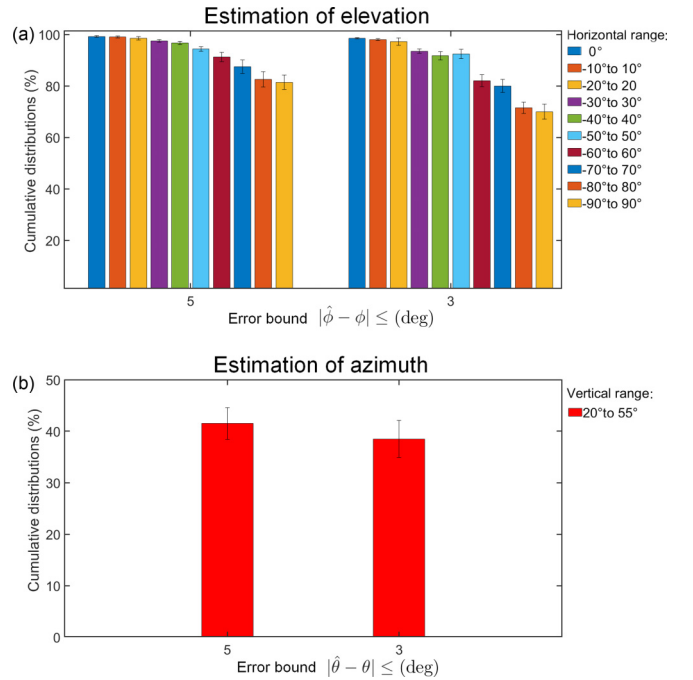


FIG. 5. Single-pulse estimation results obtained by parallel erect pinnae. The horizontal axes of (a) and (b) represent the error boundaries for counting the estimated results. (a) The mean and standard deviation of cumulative distributions in the eight cross-validation cycles for elevation estimation. The different bar colors stand for different limited scopes ranging from $\pm 0^\circ$ to $\pm 90^\circ$ of azimuth for the data. (b) The mean and standard deviation of cumulative distributions in the eight cross-validation cycles for azimuth estimation. The data came from a unique limited scope in the vertical direction, which was 20° to 55° .

the elevation results, thereby indicating that the changes in features with azimuth showed less regularity than those with elevation.

With parallel erect pinnae, elevation estimation can achieve better accuracy. These results indicated that although the SNR was poor at high elevations or at marginal azimuth, the correlations between the sweeping frequency and elevation were strongly maintained. However, the results for azimuth estimation were poor [Fig. 5(b)]. The inclusion of additional binaural information such as the interaural time difference (ITD) [22] and interaural level difference (ILD) [23] may be needed to improve the azimuthal estimate of the target.

This study did not apply binaural cues such as ITD or ILD as complementary for the azimuthal estimate of the target, but instead changed the relative topological angle of the binaural from parallel to orthogonal [Figs. 2(a)–2(c)]. In either of these two orthogonal directions, a single BP neural network with a single output can be used to make the estimate. The two neural networks have the same structure [20], which is used for the corresponding training and estimation task and after training, only the parameters of which may be different.

The estimation results of single pulse for orthogonal pinnae are shown in Figs. 6(a) and 6(b), in which the up and low bounds of each box are close to the true values, meaning that both elevation and azimuth estimation methods achieved good results. The standard deviations of both the elevation and azimuth results remained sufficiently stable at various angles. These results demonstrate that elevation and azimuth estimation can be performed simultaneously with orthogonal pinnae, although the accuracy was slightly lower than with parallel erect pinnae.

In practical applications, the specific direction of the target is of greater concern than the accuracy in one dimension, or in other words, it is hoped that the azimuth and the elevation angle of the target can be correctly estimated at the same time. Figure 6(c) shows the joint cumulative distributions for the common errors of azimuth and elevation and under pulse trains with different numbers of observations. Within these results, fewer than 80% of the estimates met the conditions of an error $|\hat{\theta} - \theta| \leq 5^\circ$ and $|\hat{\phi} - \phi| \leq 5^\circ$ simultaneously [Fig. 6(c), first bar in the second group]. Comparing the results of single pulse with pulse trains in Fig. 6(c), obviously, pulse trains can attain more accurate localization. This conclusion made from Fig. 6(c) is consistent with the behavior pattern of bat sonar. Bats always emit multiple groups of pulses (pulse trains) to search for prey [24], and using a pulse train rather than a single pulse effectively improves estimation accuracy. The mechanism of how bats use pulse trains has not been fully revealed. For artificial batlike sonar, how to use a pulse train reasonably to improve estimation of target direction is also a challenging topic. The number of pulses needed by a bat for target direction estimation is related to accuracy and sensitivity requirements [25]. The more observations, the higher the accuracy can be, but the sensitivity will decrease. In pattern recognition applications, one common idea is to use the majority decision to improve the final results. However, in this study, the output of a BP neural network is an angle value after regression, which is hard to apply a majority decision to directly. In this case, a majority vote-based method called SWCPE (sliding-window cumulative peak estimation) [20]

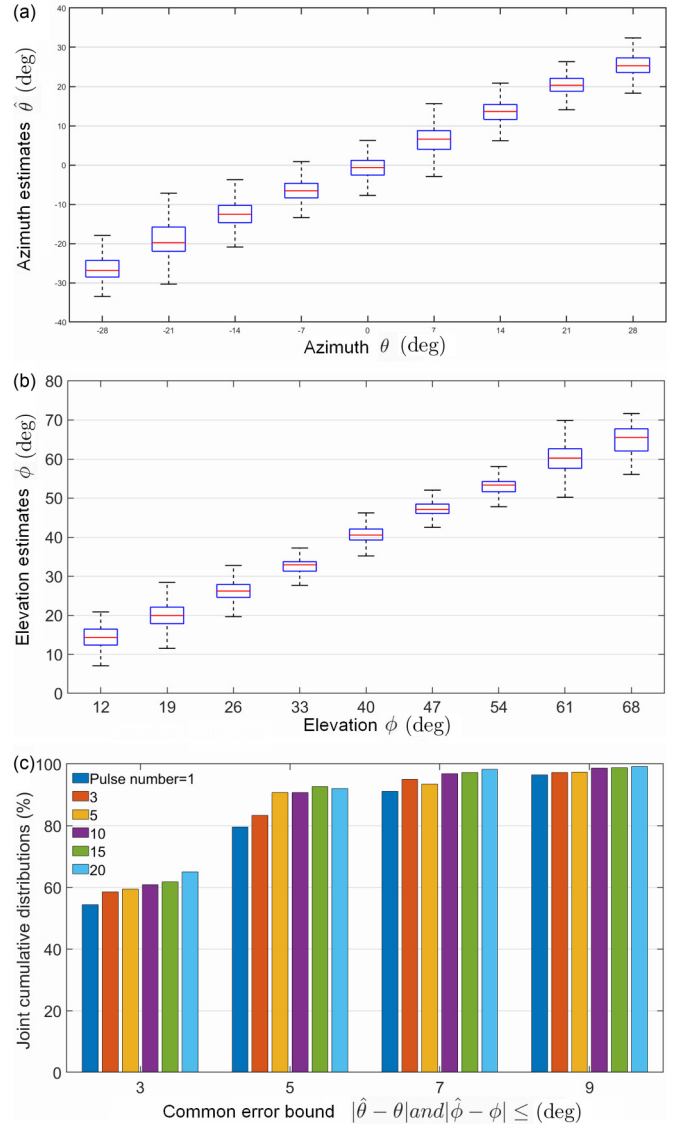


FIG. 6. Elevation and azimuth estimated with orthogonal pinnae: (a), (b) comparisons of the azimuth and elevation estimates in the single-pulse test with actual values; (c) joint cumulative distributions for the common errors of azimuth and elevation estimates under pulse trains with different numbers of observations; the abscissa axis represents the error constraint that both azimuth and elevation must meet simultaneously.

was developed to reconstruct the results. Within these results in Fig. 6(c), a pulse train containing five observations has shown a better balance between the effects of estimation and pulse number [Fig. 6(c), the third bar in each group], that is, less than 60% of all target angles were estimated with an error of $|\hat{\theta} - \theta| \leq 3^\circ$ and $|\hat{\phi} - \phi| \leq 3^\circ$ [Fig. 6(c), the third bar in the first group], but more than 91% were estimated with an error of $|\hat{\theta} - \theta| \leq 5^\circ$ and $|\hat{\phi} - \phi| \leq 5^\circ$ [Fig. 6(c), the third bar in the second group], which also shows that artificial sonar can achieve better sensitivity under the requirement for a certain accuracy.

The error constraint in the abscissa axis of Figs. 5 and 6 can also be defined as a resolution. For target localization and prey capture by echolocating bats, a very high angle resolution

can be achieved even for a farther target [26]. However, a currently rare report presents an artificial echo system that uses a strictly batlike design (using only two acoustic receivers and one acoustic emitter), which can achieve good estimation precision in practical applications. For robot target tracking, of course, the smaller the instantaneous angle error, the better the effect that will be achieved. However, the report for the radar components used for robot target tracking and target localization, which have seen wide application, presents 5° resolution over $\pm 60^\circ$ elevation and azimuth scan as being qualified for their tasks [27]. This means at least that an error of 5° is within acceptable tolerances in many practical cases. The results in this study can be treated as examples used for reference and comparison in strictly batlike research.

Big brown bats, like long-eared bats, also have a tragus, which has been found to be responsible for vertical sound localization [11,12,14]. It can be inferred that those bats that have a tragus use it for approximation in the echolocation task [16]. In addition, it can also be hypothesized from our experiments that these bats can generate direction-of-arrival estimates using only feature analysis and processing in two mutually orthogonal directions, instead of being forced to remember the features of the echo in each direction. Obviously, such behavior can make echolocation easier to achieve and

can efficiently avoid the feature confusion caused by too many classifications. The present experiment, which simulated bat species to reproduce their echolocation, can provide further insights into the true sonar mechanisms used by bats as well as serving as a validation method. In addition to the direct application of this method to the recognition of a single target by artificial bats, it can also provide a preliminary estimate before subsequently obtaining more accurate estimates. Multitarget direction estimation and sonar imaging based on a strictly batlike system will be more challenging, and this will also be considered in future research.

ACKNOWLEDGMENTS

This work was supported by the National Natural Science Foundation of China (Grant No. 61271453), the Shenzhen Science and Technology Research and Development Funds (Grant No. JCYJ20170818104011781), and the Key Research and Development Program of Shandong Province (Grants No. 2017GGX10113 and No. 2019GGX101063). The work of Z.D. was supported in part by the Fundamental Research Funds of Shandong University. We also thank all the anonymous reviewers for their helpful and stimulating comments on earlier versions of this Rapid Communication.

-
- [1] J. J. Rosowski, *Outer and Middle Ears* (Springer, New York, 1994).
 - [2] C. Bou Mansour, E. Koreman, J. Steckel, H. Peremans, and D. Vanderelst, Avoidance of non-localizable obstacles in echolocating bats: A robotic model, *PLoS Comput. Biol.* **15**, e1007550 (2019).
 - [3] R. Kuc, Generating cognitive maps using echo features from a biomimetic audible sonar, *J. Acoust. Soc. Am.* **145**, 2084 (2019).
 - [4] K. Kugler and L. Wiegrebe, Echo-acoustic scanning with noseleaf and ears in phyllostomid bats, *J. Exp. Biol.* **220**, 2816 (2017).
 - [5] M. J. Wohlgemuth, J. Luo, and C. F. Moss, Three-dimensional auditory localization in the echolocating bat, *Curr. Opin. Neurobiol.* **41**, 78 (2016).
 - [6] Y. Yamada, K. Ito, A. Oka, S. Tateiwa, T. Ohta, R. Kobayashi, S. Hiryu, and Y. Watanabe, Obstacle-avoidance navigation by an autonomous vehicle inspired by a bat biosonar strategy, in *Biomimetic and Biohybrid Systems*, Lecture Notes in Computer Science (Springer, New York, 2015), Chap. 14, pp. 135–144.
 - [7] R. Kuc, Morphology suggests noseleaf and pinnae cooperate to enhance bat echolocation, *J. Acoust. Soc. Am.* **128**, 3190 (2010).
 - [8] B. Lawrence and J. Simmons, Echolocation in bats: The external ear and perception of the vertical positions of targets, *Science* **218**, 481 (1982).
 - [9] R. Müller, A. K. Gupta, H. Zhu, M. Pannala, U. S. Gillani, Y. Fu, P. Caspers, and J. R. Buck, Dynamic Substrate for the Physical Encoding of Sensory Information in Bat Biosonar, *Phys. Rev. Lett.* **118**, 158102 (2017).
 - [10] Q. Zhuang and R. Müller, Numerical study of the effect of the noseleaf on biosonar beamforming in a horseshoe bat, *Phys. Rev. E* **76**, 051902 (2007).
 - [11] J. M. Wotton, T. Haresign, and J. A. Simmons, Spatially dependent acoustic cues generated by the external ear of the big brown bat, *Eptesicus fuscus*, *J. Acoust. Soc. Am.* **98**, 1423 (1995).
 - [12] J. M. Wotton and J. A. Simmons, Spectral cues and perception of the vertical position of targets by the big brown bat, *Eptesicus fuscus*, *J. Acoust. Soc. Am.* **107**, 1034 (2000).
 - [13] J. M. Wotton, T. Haresign, M. J. Ferragamo, and J. A. Simmons, Sound source elevation and external ear cues influence the discrimination of spectral notches by the big brown bat, *Eptesicus fuscus*, *J. Acoust. Soc. Am.* **100**, 1764 (1996).
 - [14] R. Müller, A numerical study of the role of the tragus in the big brown bat, *J. Acoust. Soc. Am.* **116**, 3701 (2004).
 - [15] C. Chiu and C. F. Moss, The role of the external ear in vertical sound localization in the free flying bat, *Eptesicus fuscus*, *J. Acoust. Soc. Am.* **121**, 2227 (2007).
 - [16] R. Müller, H. Lu, and J. R. Buck, Sound-Diffracting Flap in the Ear of a Bat Generates Spatial Information, *Phys. Rev. Lett.* **100**, 108701 (2008).
 - [17] J. M. Wotton and R. L. Jenison, A backpropagation network model of the monaural localization information available in the bat echolocation system, *J. Acoust. Soc. Am.* **101**, 2964 (1997).
 - [18] F. Schillebeeckx, F. D. Mey, D. Vanderelst, and H. Peremans, Biomimetic sonar: Binaural 3D localization using artificial bat pinnae, *Int. J. Robotics Res.* **30**, 975 (2010).
 - [19] F. Hlawatsch and F. Auger, *Time-Frequency Analysis* (Wiley, Hoboken, NJ, 2008).
 - [20] See Supplemental Material at <http://link.aps.org/supplemental/10.1103/PhysRevE.102.040401> for more details of the neural network employed in our experiments as well as details of the sliding-window cumulative peak estimation (SWCPE), which is employed in the multipulse experiments.

- [21] C. M. Bishop, *Neural Networks for Pattern Recognition* (Oxford University Press, New York, 1996).
- [22] M. Raspaud, H. Viste, and G. Evangelista, Binaural source localization by joint estimation of ILD and ITD, *IEEE Trans. Audio, Speech, Language Process.* **18**, 68 (2010).
- [23] S. T. Birchfield and R. Gangishetty, Acoustic localization by interaural level difference, in *Proceedings of the IEEE International Conference on Acoustics, Speech, and Signal Processing (ICASSP '05)* (IEEE, New York, 2005).
- [24] H.-U. Schnitzler and E. K. Kalko, Echolocation by insect-eating bats, *Bioscience* **51**, 557 (2001).
- [25] T. Hagino, S. Hiryu, S. Fujioka, H. Riquimaroux, and Y. Watanabe, Adaptive sonar sounds by echolocating bats, in *Proceedings of the 5th International Symposium on Underwater Technology, 2007 Symposium on Underwater Technology and Workshop on Scientific Use of Submarine Cables and Related Technologies* (IEEE, New York, 2007), Vols. 1 and 2, pp. 647–651.
- [26] S. Kim, Bio-inspired engineered sonar systems based on the understanding of bat echolocation, in *Biomimetic Technologies* (Elsevier, Amsterdam, 2015), pp. 141–160.
- [27] D. Guermandi, Q. Shi, A. Dewilde, V. Derudder, U. Ahmad, A. Spagnolo, I. Ocket, A. Bourdoux, P. Wambacq, and J. A. Craninckx, A 79-GHz 2×2 MIMO PMCW radar SoC in 28-nm CMOS, *IEEE J. Solid-State Circ.* **52**, 2613 (2017).